Engineered Science
DOI: https://dx.doi.org/10.30919/es1552

An Improved Bidirectional Cartesian Scanning Trajectory Formula for Ensuring Continuity and Specifying the Optimal Phase Angle for Maximum Density Pattern

Azamat Mukhatov,[1] Ton Duc Do[1,*] and Tri T. Pham[2,*]

Abstract

In this paper, we address the current issues of the traditional bidirectional Cartesian (BC) scanning trajectory when N_P, the frequency ratio and integer coefficient, is two times an odd number. Low scanning density and discontinuous waveforms are introduced by the conventional formula when the phase angle is not properly chosen. We proposed a new and better formula for ensuring continuity and specifying the phase angle for optimal scanning density. To maximize the density pattern for all N_p values, set φ=0 for $N_P/2$=even and $\varphi=\pi/2$ for $N_P/2$=odd cases. The new formula adjusts the mathematical expressions for the waveforms of the current in the driving coils in both *x* and *y* directions. The major correction ensures a smooth transition of the trajectory by preserving the continuity between the two halves of the waveform, which are switched at half of the repeat period. Quantification of pattern density and quality of magnetic particle imaging reconstructed images demonstrated that the new formula is simple to use and provides consistent performance and accuracy when compared to the best cases in the old formula. This improved bidirectional Cartesian trajectory formula provide a more effective and useful solution for a variety of high-precision scanning applications, including microscopy, imaging and automated inspection.

Keywords: Bidirectional cartesian; Mathematical formula; Phase angle; Continuous waveforms; Scanning density.
Received: 22 December 2024; Revised: 27 March 2025; Accepted: 04 May 2025.
Article type: Research article.

1. Introduction

The bidirectional Cartesian (BC) scanning trajectory is frequently used in many applications such as laser scanning confocal microscopy for high resolution biological imaging,[1] neuro-imaging applications,[2] additive manufacturing for precise material deposition,[3] robotic path planning for efficient automated inspections.[4] Machine learning also uses this scanning trajectory for path planning and real time control.[5] In magnetic particle imaging (MPI), this trajectory gives good spatial coverage and precise signal acquisition, better image quality for biomedical diagnostics and therapy monitoring.[6]

[1] *Department of Robotics, School of Engineering and Digital Sciences (SEDS), Nazarbayev University, Astana, 010000, Kazakhstan*
[2] *Department of Biology, School of Sciences and Humanities, Nazarbayev University, Astana, 010000, Kazakhstan*
* *Email*: doduc.ton@nu.edu.kz (T. D. Do); tri.pham@nu.edu.kz (T. T. Pham)

Magnetic particle imaging is a game changing imaging modality that uses the non linear magnetization behaviour of magnetic nanoparticles (MNPs) to deliver high resolution and real time imaging.[7,8] The effectiveness of MPI depends critically on the design of the scanning trajectory which affects spatial resolution, imaging speed and acquired image quality.[9,10] While sinusoidal Lissajous have been the standard in the field for their efficiency and uniform spatial coverage, other approaches like the bidirectional Cartesian trajectory, also known as the Cartesian improved trajectory, have several advantages that are worth considering even if not widely used as primary trajectories for MPI systems.[11]

The BC trajectory is a variation of the classical Cartesian raster scanning method with bidirectional scanning feature instead of an unidirectional sweeping. It creates a systematic, grid like pattern that is easy to sample the imaging field of view (FOV). It is important to note that unidirectional and bidirectional Cartesian scanning trajectories are not interchangeable due to their distinct functions and

characteristics. Unidirectional Cartesian scanning moves in one direction for each row or column and requires a reset to the starting edge, slower scanning time but no motion artifacts. Bidirectional Cartesian scanning employs sinusoidal waveforms for alternating movement, faster and more continuous coverage of the scanning FOV but can occasionally produce artifacts from waveform transitions. Unidirectional is ideal for precision applications whereas bidirectional with sinusoidal paths is preferable for high speed imaging.

The simplicity of BC scaning trajectory makes it more straightforward to implement compared to more complex patterns like sinusoidal or radial Lissajous which require smooth oscillatory motions. The BC trajectory is perfect for proof of concept experiments or MPI systems that prioritise ease of integration over high performance imaging.

Additionally, the BC trajectory excels in scenarios where localised imaging or small fields of view are required. Its grid like sampling reduces redundancy in certain regions and optimises resource utilization when the FOV of interest is small. This may also enable energy efficient operation in some circumstances, as reusing trajectory pathways in a controlled manner can reduce system expenditure.

However, the BC trajectory has several limitations that make it not suitable as a general purpose MPI trajectory. One of these is its inability to sweep spatial density as effectively as Lissajous trajectories. The rigid grid structure of the BC pattern results in uneven sampling density with oversampling in some areas and undersampling in others. This can lead to imaging artifacts and reduced spatial resolution, especially in applications that require high spatial detail. Sinusoidal Lissajous trajectories offer smoother, continuous and more uniform coverage, which improves overall imaging quality.[12]

Furthermore, the existing formula for the BC scanning trajectory does not define the phase angle, φ, to utilize for a specific N_p value. Users frequently use trial and error to select the phase angle that maximizes scanning pattern density. In addition, depending on the phase angle used, the switching of the bidirectional motion at half repeat time for the BC trajectory can result in a discontinuity or sudden change in direction of the drive field, causing significant stress to the system hardware components such as the drive coils, leading to increased energy consumption and frequent hardware damage. This poor feature of the BC trajectory makes it unsuitable for portable MPI systems or long imaging sessions where energy efficiency is critical. Sinusoidal and radial Lissajous trajectories with their continuous oscillations use more balanced energy and put less mechanical stress on the system hardware components.[13]

Although the irregularity of the BC scanning pattern simplifies some aspects of image reconstruction from a computational standpoint, the sample pattern's inherent repetition may result in greater processing demands. For example, eliminating redundant data or interpolating undersampled areas involves more processing resources, which can compromise real time imaging. In contrast, the inherent balance of sinusoidal Lissajous trajectories allows for more uniform data gathering and more accurate image reconstruction.[14]

Dynamic imaging scenarios such as blood flow or a beating heart highlight another weakness of the BC trajectory. An abrupt change in direction at half repeat time might cause motion artifacts and lower image quality and temporal resolution in dynamic studies. Sinusoidal Lissajous patterns, with their smooth and continuous motion, are the trajectory of choice for real-time imaging.

Despite these limitations, the BC trajectory still has its place in many applications including MPI. Its simplicity, reliability and reproducability make it suitable for focused applications where simplicity and ease of use are more important than resolution and dynamic imaging.[15]

The BC trajectory is an alternative to MPI's typical sinusoidal Lissajous patterns, with advantages in certain situations. It does not have the spatial coverage efficiency or dynamic imaging adaptability of sinusoidal Lissajous trajectories, but its simplicity, structured sampling and energy saving potential make it a desirable option for specific use scenarios. Maintaining its strengths while continually addressing its weaknesses will broaden and enhance the use of this scanning tracjertory in a variety of existing applications.

This work aims to revisit the existing and commonly used BC scanning trajectory and explore its characteristics and parameters, particullarly the criterion for utilizing the correct phase angle to provide a smooth and continuous waveform. The effects of the phase angle on the scanning pattern at various N_p values, as well as the abrupt change in the waveform at half the repetition time will be investigated in greater detail. We will identify and examine the type of error, demonstrate how it affects the scanning and reconstruction outcomes, and offer an effective solution. We will demonstrate through extensive testing and validation that the improved formula offers a more reliable and consistent scanning procedure that avoids discontinuity and explicitly specifies a phase angle condition.

2. Methods

The commonly used BC scanning trajectory formula by numerous researchers in the literature is shown below:[11,12,16]

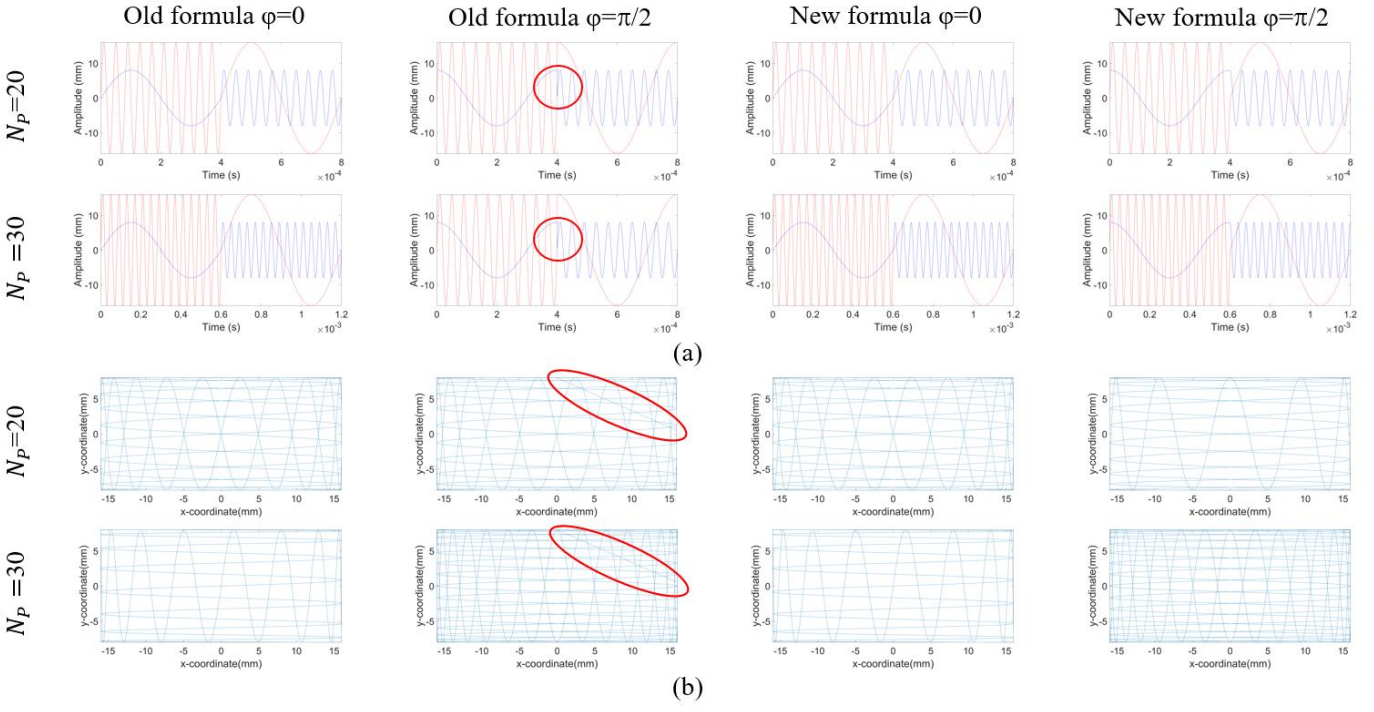

Fig. 1: (a) The generated waveforms for old and new BC formulas at different Np and phase values, and (b) their corresponding scanning patterns.

$$H_x(t) = \{Asin(2\pi f_x t), t < \frac{T_R}{2}\ Bsin\big(2\pi f_y t + \varphi\big), t \geq \frac{T_R}{2} \quad (1)$$

$$H_y(t) = \{Asin\big(2\pi f_y t + \varphi\big), t < \frac{T_R}{2}\ Bsin(2\pi f_x t), t \geq \frac{T_R}{2} \quad (2)$$

where $f_y = \frac{2f_x}{N_P}$, $T_R = \frac{N_P}{f_x}$, f_x is the fundamental frequency in x-direction, f_y is the frequency in y-direction, N_P is the integer coefficient, T_R is repetition time, φ is the phase angle, A and B are the amplitudes, and t is time.

The generated waveforms using Eqs. (1) and (2) above are demonstrated in Fig.1(a). Fig. 1(b) clearly shows that the waveforms for N_P/2=odd cases for the old formula using φ=0 setting are not optimal, as it only provides half of the pattern (*i.e.*, lower density) compared to that of the N_P/2=even cases. Setting φ=π/2 improves the pattern density in N_P/2=odd cases. However, this choice of phase angle results in a waveform discontinuity at half time, as seen by the red circles on Figure 1(a-b). This sudden changes and discontinuity in the waveforms can also put additional stress on the hardware and potentially cause damage.

To overcome these problems, we proposed a new formula for the BC scanning trajectory that maintains waveform continuity for any selected phase, which is given below:[17]

$$H_x(t) = \{Asin(2\pi f_x t), t < \frac{T_R}{2}\ Bsin\big(2\pi f_y t\big), t \geq \frac{T_R}{2} \quad (3)$$

$$H_y(t) = \{Asin\big(2\pi f_y t + \varphi\big)$$

$$t < \frac{T_R}{2}\ Bsin(2\pi f_x t + \varphi),\ t \geq \frac{T_R}{2} \quad (4)$$

The waveforms generated from Eqs. (3) and (4) above are always continuous regardless of the choice φ value used as shown in Fig. 1(a). Fig. 1(b) also clearly indicates that to achieve the maximum density pattern for all N_p values, use φ=0 for N_P/2=even and φ=π/2 for N_P/2=odd cases. Thus, the newly proposed formula ensures no discontinuity in the waveforms at half the repeat time while also providing the criterion to choose the phase angle for maximum scanning pattern density.

The improvement of the old BC scanning trajectory formula comes from phase angle φ, which previously was presented in both of the waveforms in Eqs. (1) and (2). However, it was obvious that the generated waveforms using this formula led to discontinuity and poor density scanning pattern if the phase is not adjusted properly. Therefore, Eqs. (1) and (2) were modified to include the phase only to the y-direction or the second driving waveform as shown in Eqs. (3) and (4). The outcomes presented in Fig. 1 clearly demonstrate the adtantage of the new formula over the old one, which guarantees continuity and maximum scanning density.

3. Results and discussion

To determine whether the BC scanning trajectory formula is working properly, we calculate the largest minimum and maximum distance between the six neighboring points in the

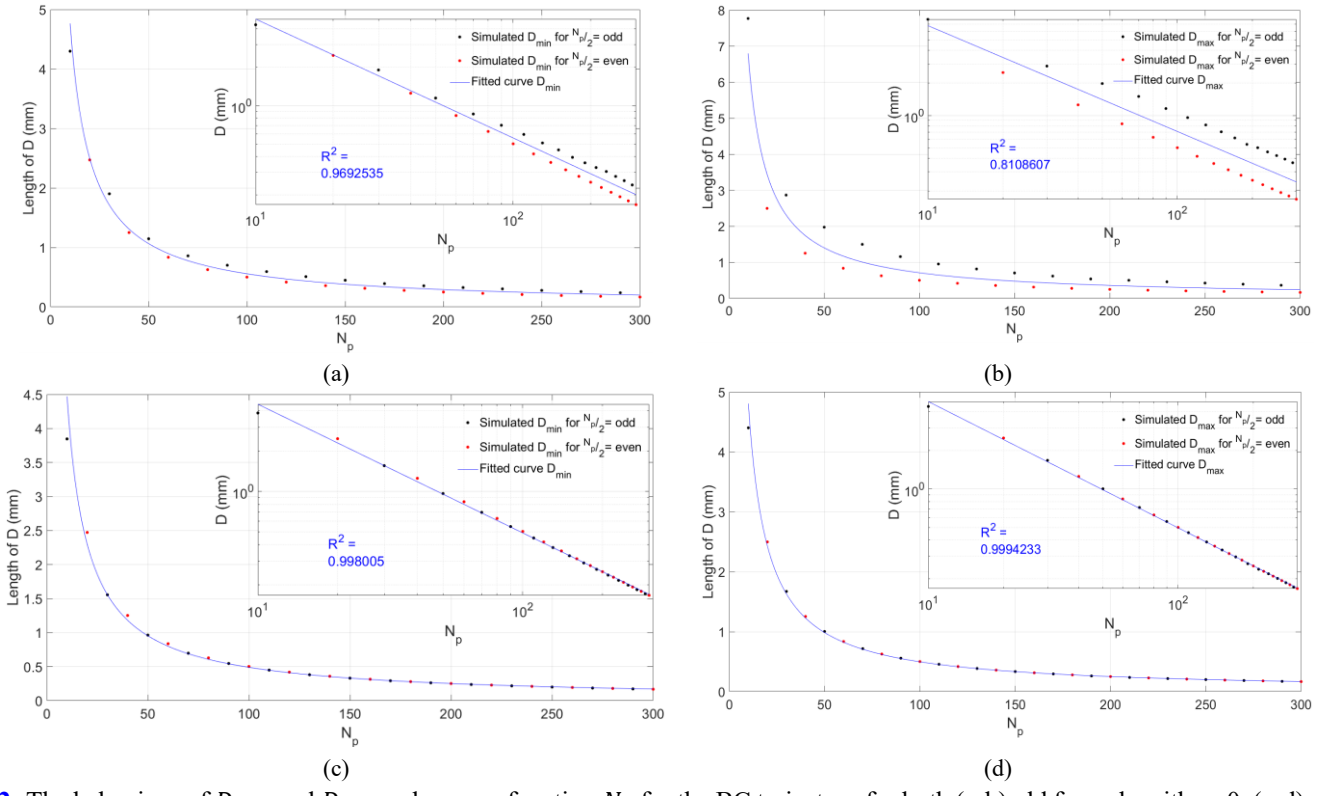

Fig. 2: The behaviour of D_{min} and D_{max} values as a function N_P for the BC trajectory for both (a-b) old formula with φ=0, (c-d) new formula with φ=0 for $N_P/2$=even and φ=π/2 for $N_P/2$=odd.

FOV as a function of N_p values. In theory, these distances should decrease as the N_p value increases because the scanning density is proportional to N_p as have been demonstrated in our previous works.[15,17] The D_{min} and D_{max} values as a function of N_p computed using the old BC trajectory formula with a fixed phase angle, φ=0, clearly demonstrate that these distances do not align with theoretical prediction. Specifically, as seen in Figs. 2(a-b), the trend for all $N_P/2$ odd cases is pushed higher in comparison to N_P /2 are even cases. According to the theory, as N_P increases, the values of H_{max}, D_{min}, and D_{max} should decrease.[15,17] However, results for $N_P/2$ are odd cases do not obey this theoretically predicted trend. As shown in Table 1, for instance, the values of the three H_{max}, D_{min}, and D_{max} distances are obviously greater for $N_P = 70$ than for $N_P = 60$. The data clearly indicate that there is an issue with the specified parameters that lead to inconsistent scanning density in the original BC scanning trajectory calculation.

The results of the newly proposed BC scanning trajectory formula demonstrate a significant improvement in both waveform continuity and maximum scanning density as shown in Fig. 1. It is worth noting that the new formula also specifies the value of the phase angle for a given N_P number based on whether $N_P/2$ is even or odd. This predefined value of the phase for a selected N_P ensures that the users get the maximum scanning density. Furthermore, the new formula also guarantees that the three H_{max}, D_{min}, and D_{max} distance values are continuously decreasing as N_p increases, as illustrated in Fig. 2 and Table 1, which is in good agreement with theoretical predictions.[15,17]

Table 1: H_{max}, D_{min} and D_{max} for N_P=60 and N_P=70.

	Old formula		New formula	
	N_P=60	N_P=70	N_P=60	N_P=70
H_{max}	0.836	1.371	0.836	0.718
D_{min}	0.836	0.860	0.836	0.697
D_{max}	0.837	1.501	0.837	0.718

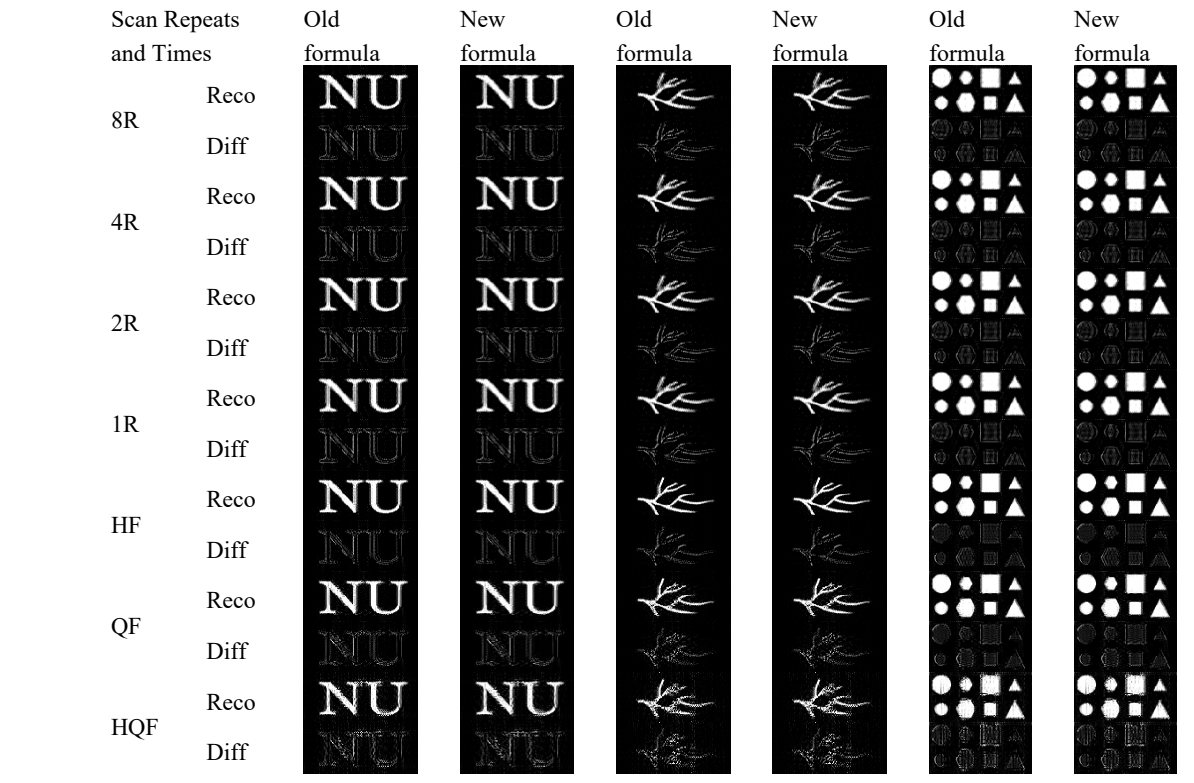

(a)

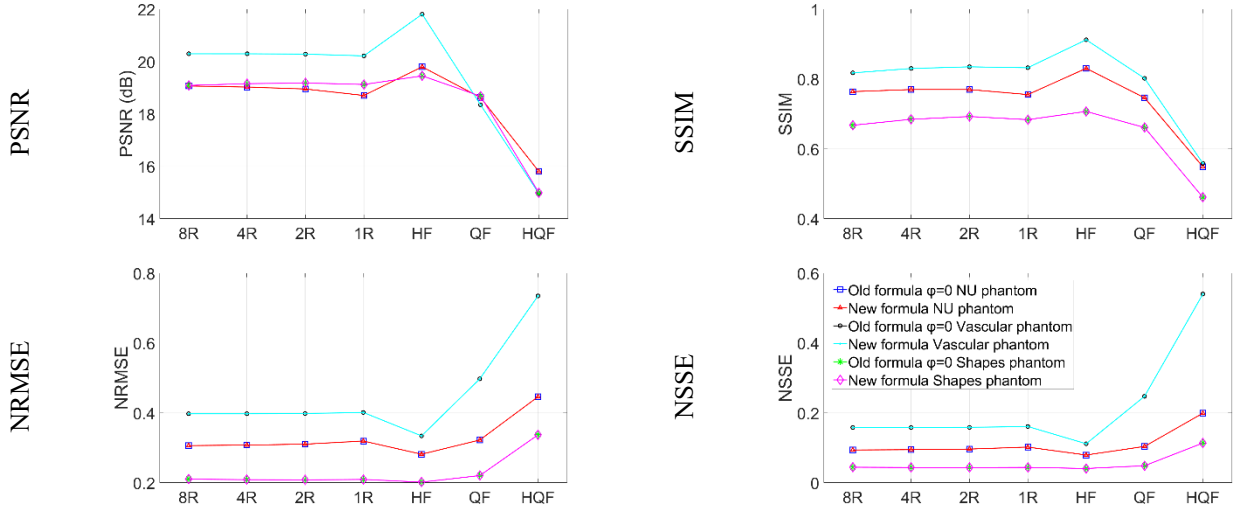

(b)

Fig. 3: (a) MPI-reconstructed images for NU, Vascular and Shapes phantoms at N_P=100 for old and new BC scanning trajectories for various cases such as 8 repeats (8R), 4 repeats (4R), 2 repeats (2R), 1 repeat (1R), Half Frequency (HF), Quarter Frequency (QF) and Half Quarter Frequency (HQF). (b) Analysis of errors for NU, Vascular and Shapes phantoms calculated for different cases such as 8R, 4R, 2R, 1R, HF, QF and HQF with N_P=100 for old and new formulas using the BC mesh.

MPI image reconstruction of NU, Vascular and Shapes phantoms was then utilized to analyze and compare the quality of old and new BC scanning trajectories. The NU phantom was named after Nazarbayev University, while the Vascular and Shapes phantoms were constructed based on similar phantoms found in the literature.[18,19] Fig. 3(a) depicts images acquired after reconstruction for various scanning repeats and times, such as 8, 4, 2, 1 repeats and half, quarter and half quarter frequencies.

Figs. 3(a-b) clearly show that there is no difference in the image reconstruction quality between old and new formulas for all $N_P/2$=even cases (*i.e.*, N_P=100). This finding reflects our prior observation for the $N_P/2$=even scenarios presented in Fig. 1. It is important to note that the results also imply that

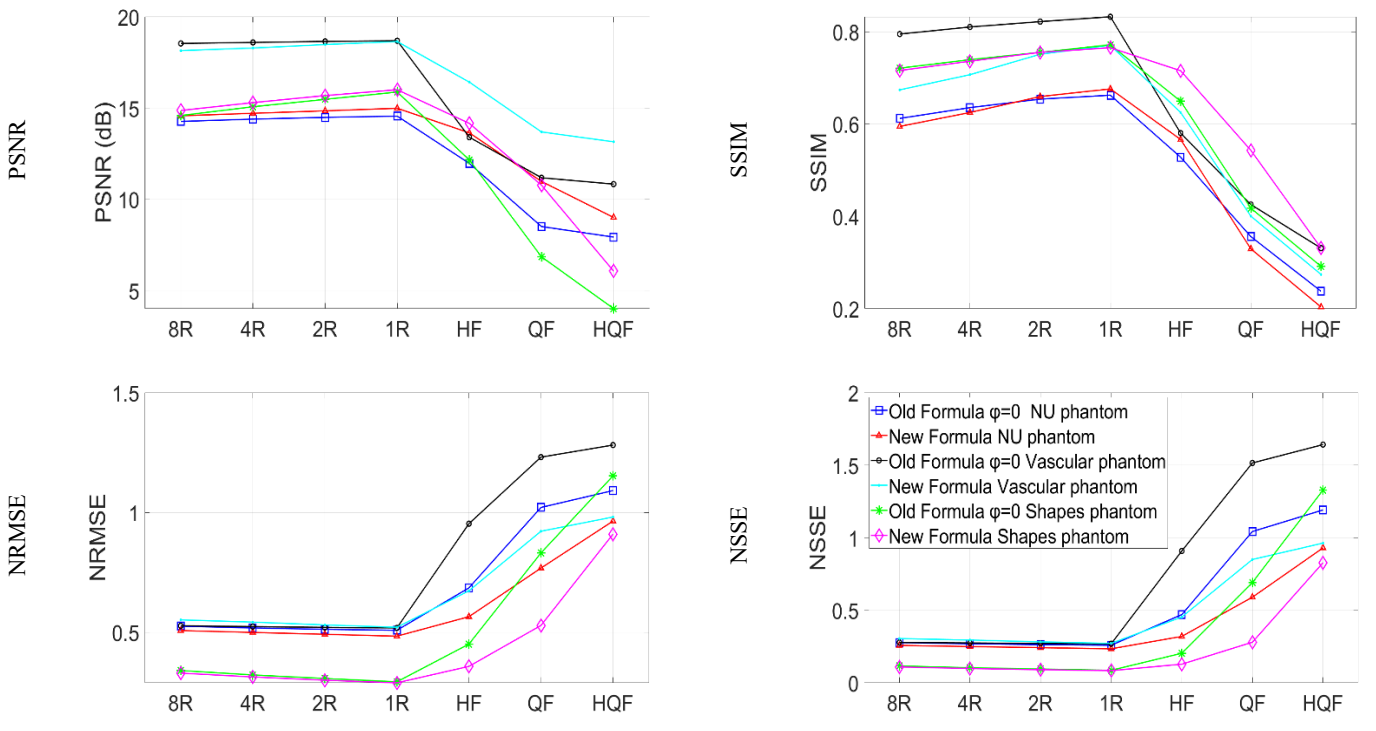
PSNR
PSNR (dB)
SSIM
SSIM
NRMSE
NRMSE
NSSE
NSSE
8R 4R 2R 1R HF QF HQF
Old Formula φ=0 NU phantom
New Formula NU phantom
Old Formula φ=0 Vascular phantom
New Formula Vascular phantom
Old Formula φ=0 Shapes phantom
New Formula Shapes phantom

(a)

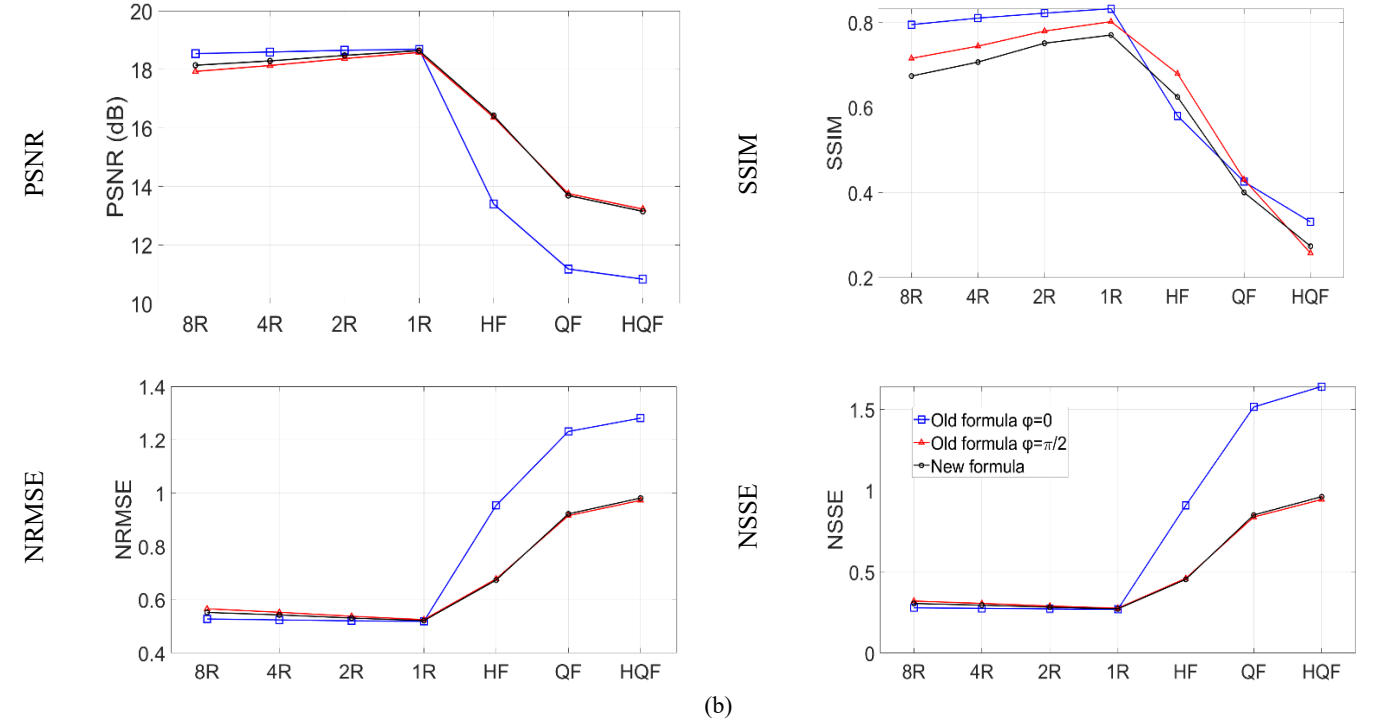
PSNR
PSNR (dB)
SSIM
SSIM
NRMSE
NRMSE
NSSE
NSSE
8R 4R 2R 1R HF QF HQF
Old formula φ=0
Old formula φ=π/2
New formula

(b)

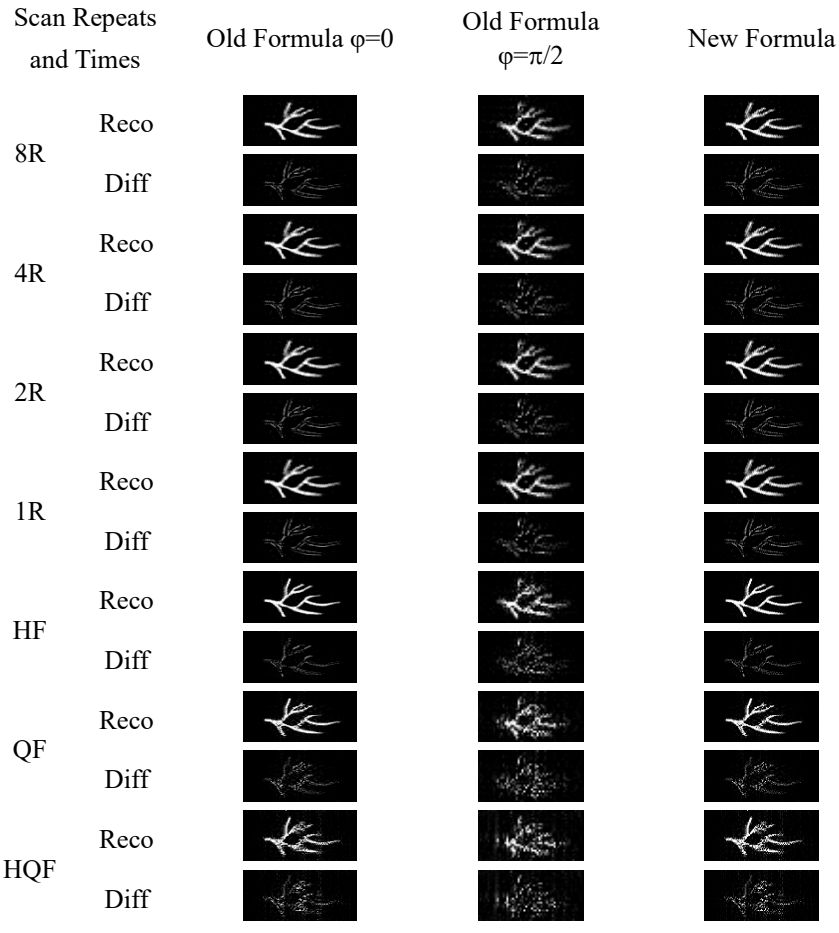

(c)

Fig. 4: (a) Analysis of NU, Vascular and Shapes phantoms calculated over several scenarios such as 8R, 4R, 2R, 1R, HF, QF and HQF of scanning for various methods with N_P=50 for BC old and new scanning trajectories at BC mesh. (b) Analysis of Vascular phantom calculated over different cases such as 8R, 4R, 2R, 1R, HF, QF and HQF of scanning for various methods with N_P=50 for BC old formulations for φ=0, φ=π/2 and new formulation scanning trajectories at BC mesh. (c) Reconstructed images of Vascular phantom.

phantoms with simple shapes will produce lower error as well as signal-to-noise and structure similarity, whereas complexed shapes, like Vascular phantom, will produce better signal-to-noise and structure similarity but also suffer from high errors, most likely due to the high amount of curved edges.

Both the old and new BC trajectory formulas were also simulated, evaluated and compared for N_P/2=odd cases, such as N_P=50. Fig. 4(a) shows that the new formula outperforms the old one on all measures while using the phase angle φ=0 for the old BC formula. The results show that the new formula has lower normalized root-mean-square and normalized sum square errors (NRMSE and NSSE), higher peak signal-to-noise ratio (PSNR) and structural similarity index measure (SSIM) values.

Simulations of the old BC trajectory formula with the phase angle φ=π/2 restored the values of the PNSR, NRSME and NSSE to those of the new formula, as shown in Fig. 4(b) for the Vascular phantom. The SSIM values for the new formula are slightly lower than those of the old formula for both phases, but the trend is the same. Changing the phase angle to π/2 for the old BC formula does not prevent discontinuity in the waveform at half the repeat period, as demonstrated in Fig. 1(a). Fig. 4(c) shows the reconstructed images and their differences from the phantom for the old BC formula with two different phases compared to the new formula.

4. Conclusion

This study reviewed the characteristics of the traditional bidirectional Cartesian scanning trajectory such as its waveform as a function of time and the scanning pattern for different N_P values. We found that there are still some problems with the traditional BC scanning trajectory that need to be fixed. First of all, the BC formula does not specify the phase angle, so it is up to the user to experiment to find the one that yields the highest

density pattern. Second, in order to get the highest scanning density pattern, the phase angle φ needs to be set to π/2 when $N_P/2$ is an odd integer. This will, however, cause a discontinuity in the waveform at half of the repeat period, which puts more strain on the hardware and could result in an early failure.

To solve these concerns, we proposed a new and improved BC scanning trajectory formula that guarantees waveform continuity and provides the phase angle that maximizes scanning density regardless of whether $N_P/2$ is odd or even. Extensive simulations and empirical validations utilizing MPI image reconstruction of various shape phantoms demonstrated that the new BC formula is not only simple to use, but it also addresses the identified issues in the traditional BC formula while maintaining the reliability and accuracy. Thus, the new BC scanning trajectory formula provides an improved and practical solution for many existing applications to reduce hardware damage and enhance the efficiency of scanning operation.

Acknowledgements

This research was funded by the Science Committee of the Ministry of Science and Higher Education of the Republic of Kazakhstan with Grant no. AP23489542 and the Grant title 'Enhancing Magnetic Particle Imaging System Sensitivity and Image Quality for Targeted Cancer Diagnosis and Treatment'.

Conflict of interest

There is no conflict of interest.

Supporting Information

Not applicable.

References

[1] A. Žemaitis, M. Gaidys, M. Brikas, P. Gečys, G. Račiukaitis, M. Gedvilas, Advanced laser scanning for highly-efficient ablation and ultrafast surface structuring: experiment and model, *Scientific Reports*, 2018, **8**, 17376, doi: 10.1038/s41598-018-35604-z.

[2] G. Zhu, B. Jiang, L. Tong, Y. Xie, G. Zaharchuk, M. Wintermark, Applications of deep learning to neuro-imaging techniques, *Frontiers in Neurology*, 2019, **10**, 869, doi: 10.3389/fneur.2019.00869.

[3] J. Lettori, R. Raffaeli, P. Bilancia, M. Peruzzini, M. Pellicciari, A review of geometry representation and processing methods for Cartesian and multiaxial robot-based additive manufacturing, *The International Journal of Advanced Manufacturing Technology*, 2022, **123**, 3767-3794, doi: 10.1007/s00170-022-10432-8.

[4] C. Mineo, S. G. Pierce, B. Wright, P. I. Nicholson, I. Cooper, Robotic path planning for non-destructive testing of complex shaped surfaces, *41ST Annual Review of Progress in Quantitative Nondestructive Evaluation*, Boise, Idaho, AIP Publishing LLC, 2015, **34**, 1977-1987, doi: 10.1063/1.4914825.

[5] A. Diveev, E. Sofronova, N. Konyrbaev, S. Ibadulla, Stabilisation system synthesis for motion along the trajectory by evolutionary machine learning control, *Engineered Science*, 2024, **29**, 1130, doi: 10.30919/es1130.

[6] T. D. Do, A. Mukhatov, A. Tolebay, T. A. Le, T. T. Pham, A comprehensive analysis of the impacts of Image Resolution and Scanning Times on the quality of MPI-reconstructed images, *Scientific Reports*, 2025, **15**, 5519, doi: 10.1038/s41598-025-89296-3.

[7] T. Knopp, N. Gdaniec, M. Möddel, Magnetic particle imaging: from proof of principle to preclinical applications, *Physics in Medicine & Biology*, 2017, **62**, R124, doi: 10.1088/1361-6560/aa6c99.

[8] A. C. Bakenecker, M. Ahlborg, C. Debbeler, C. Kaethner, T. M. Buzug, K. Lüdtke-Buzug, Magnetic particle imaging in vascular medicine, *Innovative Surgical Sciences*, 2018, **3**, 179-192, doi: 10.1515/iss-2018-2026.

[9] M. Grosser, M. Möddel, T. Knopp, Using low-rank tensors for the recovery of MPI system matrices, *IEEE Transactions on Computational Imaging*, 2020, **6**, 1389-1402, doi: 10.1109/TCI.2020.3024078.

[10] J. Franke, N. Baxan, H. Lehr, U. Heinen, S. Reinartz, J. Schnorr, M. Heidenreich, F. Kiessling, V. Schulz, Hybrid MPI-MRI system for dual-modal in situ cardiovascular assessments of real-time 3D blood flow quantification-a pre-clinical in vivo feasibility investigation, *IEEE Transactions on Medical Imaging*, 2020, **39**, 4335-4345, doi: 10.1109/TMI.2020.3017160.

[11] T. Knopp, S. Biederer, T. Sattel, J. Weizenecker, B. Gleich, J. Borgert, T. M. Buzug, Trajectory analysis for magnetic particle imaging, *Physics in Medicine and Biology*, 2009, **54**, 385-397, doi: 10.1088/0031-9155/54/2/014.

[12] A. A. Ozaslan, A. Alacaoglu, O. B. Demirel, T. Çukur, E. U. Saritas, Fully automated gridding reconstruction for non-Cartesian x-space magnetic particle imaging, *Physics in Medicine & Biology*, 2019, **64**, 165018, doi: 10.1088/1361-6560/ab3525.

[13] D. Boiroux, Y. Oke, F. Miwakeichi, Y. Oku, Pixel timing correction in time-lapsed calcium imaging using point scanning microscopy, *Journal of Neuroscience Methods*, 2014, **237**, 60-68, doi: 10.1016/j.jneumeth.2014.08.008.

[14] F. Werner, N. Gdaniec, T. Knopp, First experimental comparison between the Cartesian and the Lissajous trajectory for magnetic particle imaging, *Physics in Medicine & Biology*, 2017, **62**, 3407, doi: 10.1088/1361-6560/aa6177.

[15] A. Mukhatov, T. A. Le, T. T. Pham, T. D. Do, A comprehensive review on magnetic imaging techniques for biomedical applications, *Nano Select*, 2023, **4**, 213-230, doi: 10.1002/nano.202200219.

[16] P. Szwargulski, M. Ahlborg, C. Kaethner, T. M. Buzug, Trajectory analysis using static patches for magnetic particle imaging, *IEEE Transactions on Magnetics*, 2015, **51**, 6501104, doi: 10.1109/TMAG.2014.2350152.
[17] A. Mukhatov, T. Le, T. D. Do, T. T. Pham, Universal behavior of the image resolution for different scanning trajectories, *Applied System Innovation*, 2023, **6**, 103, doi: 10.3390/asi6060103.
[18] P. W. Goodwill, J. J. Konkle, B. Zheng, E. U. Saritas, S. M. Conolly, Projection X-space magnetic particle imaging, *IEEE Transactions on Medical Imaging*, 2012, **31**, 1076-1085, doi: 10.1109/TMI.2012.2185247.
[19] K. Murase, Simultaneous correction of sensitivity and spatial resolution in projection-based magnetic particle imaging, *Medical Physics*, 2020, **47**, 1845-1859, doi: 10.1002/mp.14056.